Springer

KSME

Journal of Mechanical Science and Technology 31 (11) (2017) 5477~5483
www.springerlink.com/content/1738-494x(Print)/1976-3824(Online)
DOI 10.1007/s12206-017-1042-z

Design for additive manufacturing of customized cast with porous shell structures †

Yeong-Eun Lim, Na-Hyun Kim, Hye-Jin Choi and Keun Park*

Department of Mechanical System Design Engineering, Seoul National University Science and Technology, Seoul 01811, Korea

(Manuscript Received May 1, 2017; Revised July 13, 2017; Accepted July 16, 2017)

Abstract

Additive manufacturing (AM) recently has been changing from conventional Rapid prototyping (RP) to direct fabrication of functional parts. As a direct fabrication method, a promising application of AM is to make personalized or customized parts; biomedical applications customized to human's bodies can provide improved functionalities for an example. In this study, a customized plastic cast is developed to replace traditional plaster casts. For customization, its basic shape is defined out of three-dimensional (3d) scan data of a human arm. This cast is designed to have a number of holes for lighter weight and better ventilation, and to be printed using a Material extrusion (ME) type 3d printer that uses thermoplastic polymer filaments. Finite element (FE) analyses are then performed to evaluate the structural safety and stiffness of the printed cast with porosity. Considering that the structural safety and stiffness are degenerated due to the porous structure, design reinforcements are suggested to improve the bending stiffness of the porous cast. FE analyses are then performed with variations of design parameters of the reinforcement structures, from which we obtain the best design candidate that provides higher specific stiffness than the conventional solid structure. A porous-customized cast with lighter weight and better ventilation can thereby be developed successfully.

Keywords: Additive manufacturing; Customized cast; Finite element analysis; Lightweight structure; 3d printing

1. Introduction

In recent years, Additive manufacturing (AM) has been changed from conventional Rapid prototyping (RP) to direct fabrication of functional parts [1]. As a direct fabrication method, a promising application of AM is to fabricate personalized or customized parts. Such biomedical applications customized to human bodies can offer improved functionalities [2]. Among the biomedical applications, orthoses are attracting attention as a useful application of AM because they can lend greater performance when they are fabricated to fit the bodies of patients [3].

Orthoses are assistive devices to help disabled or injured people, and are used to support human musculoskeletal systems. Fracture orthoses, also known as casts or splints, are used to protect musculoskeletal injuries such as sprains, dislocations, and bone fractures by preventing motion of the injured parts. At the beginning of orthopedic treatment, in general, a splint is temporarily used to prevent motion of the injured part to some extent while its open structure allows natural swelling of the injured region. A circumferential casting is then used to fully immobilize the injured part after the swelling has subsided [4].

*Corresponding author. Tel.: +82 2 970 6358, Fax.: +82 2 974 8270
E-mail address: kpark@seoultech.ac.kr
† Recommended by Editor Haedo Jeong

In the past decade, AM has been used to fabricate customized orthoses including ankle-foot [5-7] and wrist-hand orthoses [8-12] for the purpose of replacing traditional plaster casts. While Ankle-foot orthoses (AFO) are designed to have a simple shell shape that covers the back and under area of the ankle-foot, Wrist-hand orthoses (WHO) are designed to have complicated shapes for weight reduction and ventilation by virtue of intrinsic design freedoms of AM technologies [10-12].

The design freedom of AM originates from the unique layer-by-layer deposition strategy, which makes it possible to overcome constraints from the traditional manufacturing technologies. A new terminology, *Design for additive manufacturing* (DFAM), is used to differentiate this from the traditional *Design for manufacturing* (DFM) [13]. DFAM has versatile applications including cost effective production of custom-fit products, functional parts with textures and porosity, and lightweight structures with lattices or cellular materials [14, 15]. Design methodologies such as constructing cellular structures [16-18], porous structures [19, 20], and skin-frame structures [21, 22] have also been studied to realize DFAM, by utilizing AM technologies in fabricating complicated structures.

In the present study, a porous cast for an elbow orthosis is developed by utilizing the concept of DFAM. The porous cast is designed to overcome disadvantages of traditional plaster

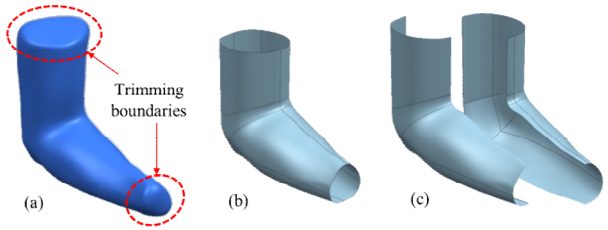

Fig. 1. Construction of 3d surface data for an arm: (a) 3d scanned point cloud data; (b) generated surface data; (c) divided surfaces.

casts, such as difficulties in donning and doffing, relatively heavy weight, and skin irritations due to poor ventilation. For this purpose, the proposed cast was designed to have a number of holes for lighter weight and better ventilation. A design procedure by effectively connecting three-dimensional (3d) scanning, automatic hole generation and 3d modeling of a pair of cast shells with reinforcement features was proposed. Finite element (FE) analyses were then performed to evaluate the structural safety and stiffness of the porous cast. From these analyses, the best design candidate was determined to ensure higher specific stiffness than the conventional solid structure. The final design was then fabricated using an extrusion type 3d printer, and the printed cast was applied to a human body successfully.

2. Design procedure of a customized cast

2.1 Surface construction from 3d scanning

To develop a customized cast, a human arm was scanned in a bent position under the assumption of an elbow injury. A hand-held type 3d scanner (Sense^{TM}, 3D Systems Inc., USA) was used to obtain a full 3d point cloud data, as shown in Fig. 1(a). The scanning data were trimmed out with respect to trimming boundaries, and then imported to 3d CAD software (Unigraphics NX8, Siemens, Germany). Surface data for the arm part were then generated based on the scanned data (Fig. 1(b)), and were divided into two parts for assembly (Fig. 1(c)). These surface data will be used in the further design processes, as described in the following sections.

2.2 Automatic generation of porous shell structure

The proposed porous shell structure contains a number of holes for the purpose of weight reduction and ventilation improvement. To generate such a porous shell efficiently, an automatic hole generation algorithm was developed for the prepared surface. The detailed procedure is given as follows: (i) Definition of a target surface for hole generation; (ii) discretization of the target surface based on FE mesh generation; (iii) generation of a number of spheres at every nodal point; (iv) Boolean operation to subtract every sphere from the target surface. Fig. 2 illustrates this procedure as a flowchart.

To apply the automatic hole generation based on FE mesh data, ANSYS APDL (ANSYS parametric design language,

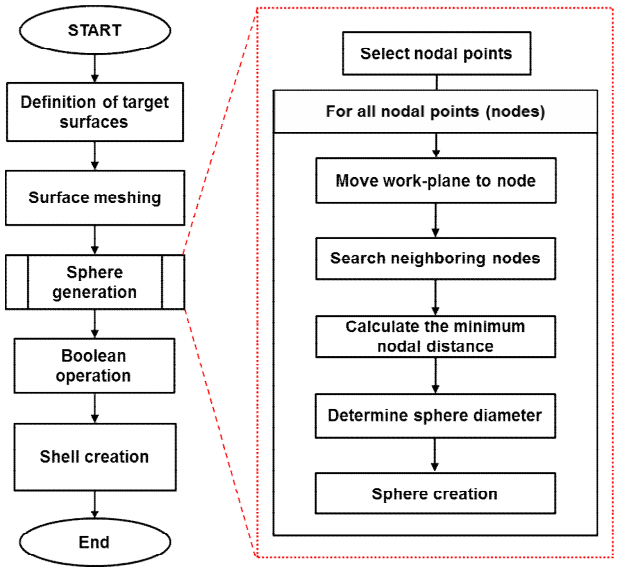

Fig. 2. Flowchart for the automatic hole generation procedure.

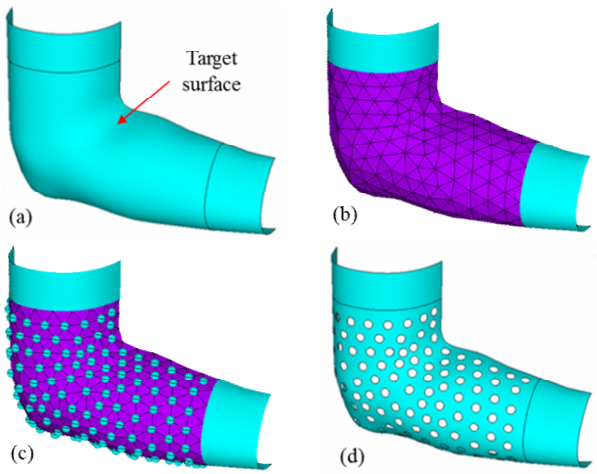

Fig. 3. Automatic hole generation procedure: (a) Definition of the target surface; (b) mesh generation for the target surface; (c) sphere creation at nodal points; (d) Boolean operation to generate a porous surface.

ANSYS Inc., USA) was used. A half surface was loaded in the ANSYS APDL environment, and was partitioned to distinguish the target surface from the remaining area. Fig. 3(a) shows the partitioned result, where the two end regions were excluded from hole generation. Fig. 3(b) shows the generated surface mesh that consists of 161 nodal points and 260 triangular elements. In this stage, FE mesh should be generated as uniform as possible so that the most triangles should be shaped equilaterally.

A number of spheres were then created at every nodal point, as shown in Fig. 3(c), except for the nodes on the boundary curves. Here, the sphere diameter was set automatically in order to avoid overlap of adjacent holes. Fig. 3(d) shows the porous surface obtained from the Boolean operation, in which all spheres were subtracted from the target surface.

Fig. 4. Design procedure of the porous cast: (a) Thickened shell; (b) additional features creation; (c) virtual assembly.

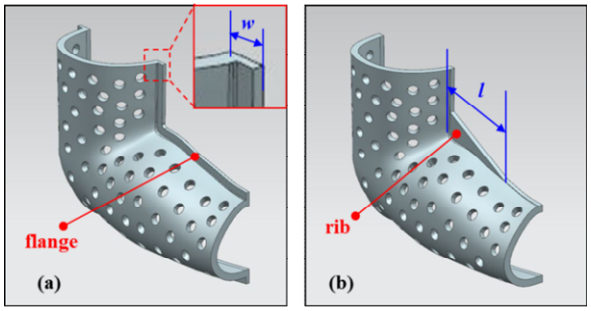

Fig. 5. Design of reinforcement features: (a) The flange reinforcement; (b) the rib reinforcement.

2.3 Design of the porous cast with reinforcement structures

The generated porous surface data were imported to CAD software, and the following design procedure was conducted to make a 3d model of the porous cast. First, a porous shell was generated by giving a thickness value to the porous surface. Fig. 4(a) shows a thickened shell that was generated by offsetting the porous surface to the outward direction with a 6 mm thickness. A pair of half casts were then prepared as shown in Fig. 4(b), with additional features for assembly and reinforcement. Fig. 4(c) shows a virtually assembled part in which both half casts were assembled to the 3d scanning data appropriately.

Although this porous cast has advantages of weight reduction and ventilation, the porosity may deteriorate the structural safety of the cast. Considering that the main function of the elbow cast is to immobilize the motion of the arm around the elbow, two reinforcement designs, flange and rib reinforcements, were proposed to increase the bending stiffness. Fig. 5(a) shows a flange reinforcement in which two flanges with 3 mm thickness were added along two parting edges. Fig. 5(b) represents a rib reinforcement in which a triangular rib with 3 mm thickness was added in the concave region of the cast. In each case, the flange width (w) and the rib length (l) were defined as design parameters. The effects of these parameters on the bending stiffness will be investigated in the following section.

3. Structural analyses of the porous cast

3.1 Overview of the structural FE analysis

To investigate the bending stiffness of porous casts according to their porosity and reinforcement structures, a structural FE analysis was performed. ANSYS Multiphysics (ANSYS Inc., USA) was used to perform the structural FE analysis for various 3d-printed cast designs.

Table 1. Orthotropic mechanical properties of printed sample [23].

Printing directions	X	Y	Z
Elastic modulus (GPa)	2.178	2.497	2.258
Tensile strength (MPa)	28.47	33.47	8.39

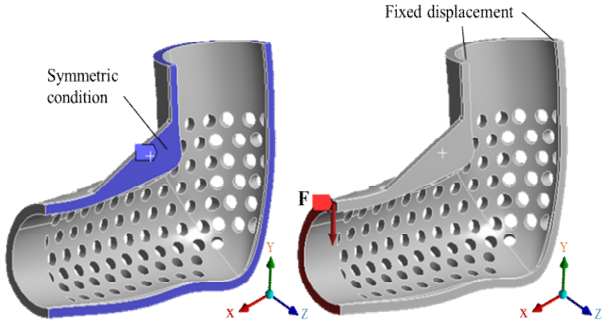

Fig. 6. Boundary conditions for structural analysis of the porous cast.

In this study, the porous casts were printed using an extrusion type 3d printer. Acrylonitrile butadiene styrene (ABS) filaments of 1.75 mm diameter (Shenzhen Esun Industrial Co. Ltd., China) were used as printing material. According to a previous study by the authors [23], 3d-printed parts using this filament have orthotropic tensile properties, as shown in Table 1. These orthotropic properties were then used in the structural FE analysis.

Fig. 6 represents boundary conditions for the FE analysis with coordinate information. Considering that 3d-printed parts show deteriorated mechanical properties along the lamination direction, the cast was designed to be laminated along the Z-direction; parting surfaces were located on the XY-plane thereby. For these parting surfaces, symmetric boundary conditions were given by constraining normal displacements of the surfaces. The upper end face (shoulder side) was fixed, and a downward force of 100 N was imposed on the lower end face (wrist side).

To investigate the bending stiffness quantitatively according to the porosity, a specific bending stiffness (k*) was defined as follows:

$$k = \frac{1}{m}\frac{F}{\delta_{\max}} \tag{1}$$

where m is the mass of a cast, F is the external force, and δ_{max} is the corresponding maximum vertical displacement, respectively. Indeed, a higher specific stiffness means a better stiffness-to-mass ratio, which is the main goal of lightweight structures.

Table 2. Comparison of FE analysis results for various shell designs.

t (mm)	D (mm)	δ_{max} (mm)	m (g)	k^* (N/g-mm)
5.0	8.0	1.462	123.7	0.553
5.0	10.0	1.977	109.5	0.462
6.0	8.0	1.040	150.5	0.639
6.0	10.0	1.372	133.5	0.546
Solid shell		0.855	152.7	0.766
Triangular net		2.243	187.4	0.238

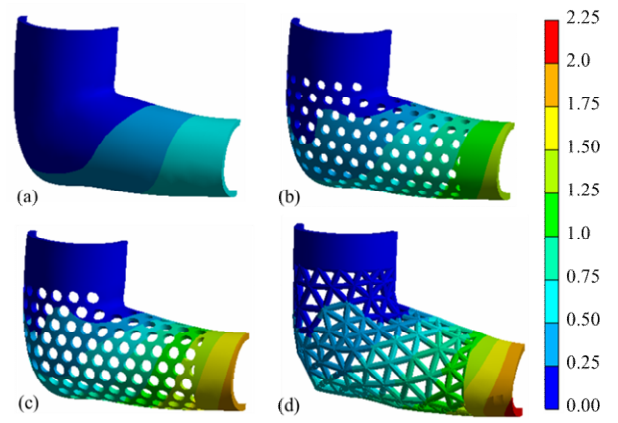

Fig. 7. Comparison of vertical displacement (unit: mm) for various structures: (a) Without hole; (b) 8 mm hole; (c) 10 mm hole; (d) triangular net structure.

3.2 Effect of porosity

Structural FE analyses were performed to investigate the effect of porosity on the bending stiffness. As a reference solution, a solid shell without holes was also analyzed and compared. The shell thickness was 5.0 mm, and the resulting vertical displacement distribution is shown in Fig. 7(a). The maximum displacement was 0.855 mm, and the corresponding specific stiffness was calculated to be 0.766 N/g-mm. Figs. 7(b) and (c) show the displacement distributions of the porous casts with hole diameters of 8 and 10 mm, respectively. It can be seen that the maximum displacements increased as the hole diameter increased: 1.462 mm for the 8 mm hole and 1.977 mm for the 10 mm hole.

To compare the bending stiffness of the porous structure with the previous net structure [11, 12], a triangular net structure was also analyzed, as shown in Fig. 7(d). The triangular net structure was constructed using the surface mesh information in Fig. 3(b); it was also generated automatically by creating a number of cylinders with 6 mm diameters for all triangular edges. The maximum deformation was 2.243 mm, which was much larger than those of porous structures.

For a quantitative comparison of the bending stiffness, porous shell structures were analyzed with variations in the shell thickness (t) and hole diameter (D). The relevant results are summarized in Table 2, in which the results for the solid shell and triangular structure are also included for comparison. Overall, the specific bending stiffness of the porous structures was lower than that of the solid shell, but higher than that of the triangular net structure. Among the four design cases of the porous shells, the third case (t = 6.0 mm, D = 8.0 mm) showed the largest specific stiffness (0.639 N/g-mm), while this value was still lower than that of the solid shell (0.766 N/g-mm).

Table 3. Comparison of FE analysis results according to flange width.

w (mm)	δ_{max} (mm)	m (g)	k^* (N/g-mm)
0	1.040	150.5	0.639
4	0.975	156.9	0.654
6	0.934	159.6	0.671
8	0.893	162.8	0.688

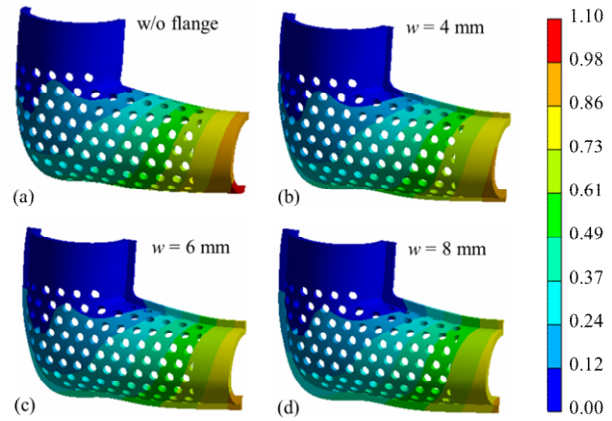

Fig. 8. Comparison of vertical displacement (unit: mm) for various flange widths: (a) Without flange; (b) 4 mm; (c) 6 mm; (d) 8 mm.

3.3 Effect of the flange width (w)

To investigate the effect of flange reinforcement on the bending stiffness, structural FE analyses were performed with variation of the flange width (w): 4, 6 and 8 mm. Figs. 8(a)-(d) show the distributions of the vertical displacement for each case, and the detailed results are compared in Table 3 quantitatively. It can be seen that the maximum displacement decreased as the flange width increased, while the part mass also increased on the other hand. Therefore, the resulting improvement in the bending stiffness was not as significant as the reduction of displacement; the reinforcement with 8 mm flanges showed a 14.1 % reduction of displacement while the improvement of the bending stiffness was only 7.7 %. This indicates that the flange reinforcement is not an efficient lightweight structure that can provide higher bending stiffness than the solid shell structure.

3.4 Effect of the rib length (l)

In this section, the rib reinforcement is considered instead of the flange reinforcement. Structural FE analyses were performed with variation of the rib length (l): 30, 50 and 70 mm.

Table 4. Comparison of FE analysis results according to rib length.

l (mm)	δ_{max} (mm)	m (g)	k^* (N/g-mm)
0	1.040	150.5	0.639
30	0.967	151.8	0.696
50	0.842	154.4	0.769
70	0.816	155.4	0.789

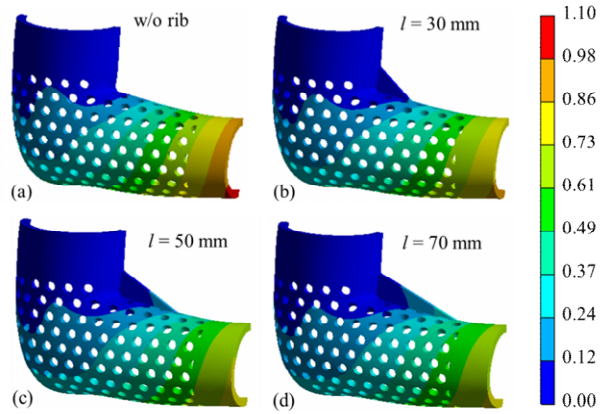

Fig. 9. Comparison of vertical displacement (unit: mm) for various rib lengths: (a) Without rib; (b) 30 mm; (c) 50 mm; (d) 70 mm.

Figs. 9(a)-(d) show the displacement distributions, and the detailed results are compared in Table 4. It can be seen that the maximum displacement also decreased as the rib length increased. The part mass showed a slight increase, but not as significant as that of the flange reinforcement case. Accordingly, the resulting improvement in the bending stiffness is more significant than the flange reinforcement cases; the specific stiffness increased to 0.789 N/g-mm in the case of 70 mm rib length, which is even higher than that of the solid shell (0.766 N/g-mm). This indicates that the rib reinforcement is more efficient than the flange reinforcement in terms of lightweight design. Based on these results, the rib reinforcement with 70 mm length was determined as the final design of the porous cast.

4. Experimental verification

4.1 Additive manufacturing of the porous cast

Based on the final design, the porous cast pairs were printed using an extrusion type 3d printer (Cubicon Single, CUBICON Inc., Korea). The nozzle and bed temperatures were set to 240 and 115 °C, respectively. The feed rate was set to 200 mm/s, and the layer thickness was set to 0.2 mm. Fig. 10(a) is a photograph of the printed cast pairs, which could be successfully worn on a human arm, as shown in Fig. 10(b). These cast pairs weigh only 155.4 g, which is lighter than the traditional plaster cast. Fig. 10(c) presents X-ray images of the casted arm in which all bones are clearly visible. Therefore, the porous cast manufactured by the thermoplastic polymer has an additional advantage in comparison with the traditional plaster cast of being transparent for X-ray so that the bone fracture status can be monitored, which was impossible with traditional plaster casts.

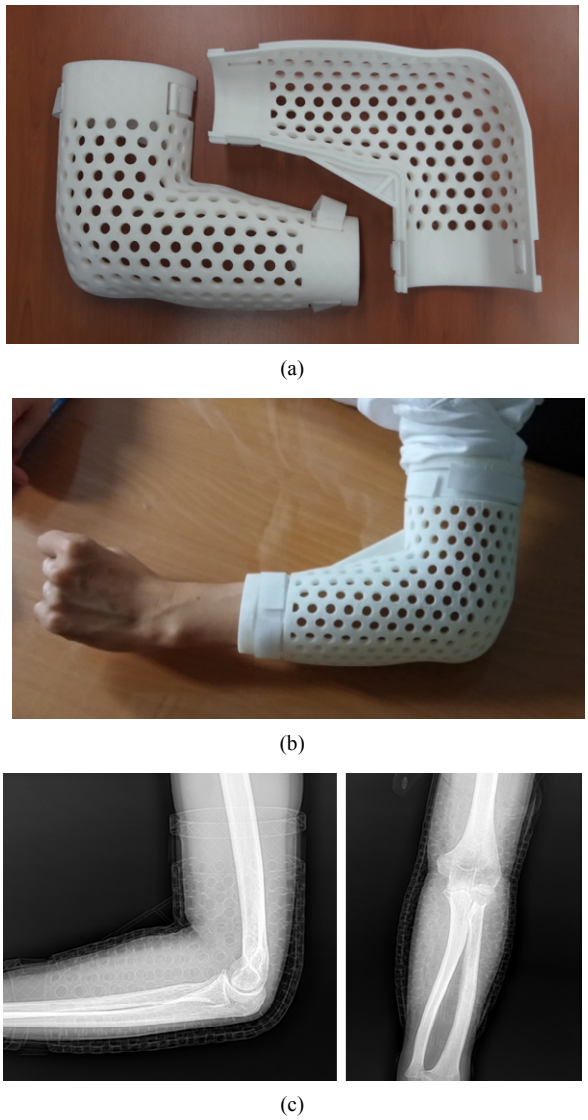

Fig. 10. Additive manufacturing of the porous cast: (a) Printed cast pairs; (b) applied to a human arm; (c) X-ray images.

4.2 Evaluation of structural safety

Compression tests were performed to evaluate the structural safety of the printed casts. To compare the 3d-printed porous cast with traditional plaster casts, a simplified half-cylindrical shell structure was prepared as shown in Fig. 11. Fig. 11(a) shows a plaster shell with an inner radius of 39 mm and a thickness of 7 mm. Fig. 11(b) shows a 3d-printed ABS shell of the same dimensions containing a number of holes. Compression tests were performed by pressing each shell, as illustrated in Fig. 11(c), and the resulting force-deformation variations were measured.

To investigate the structural safety of these shell structures, the critical force at the failure location (F_{crit}) and the compres-

Table 5. Comparison of the critical force and stiffness.

Material	Plaster	ABS
Mass (g)	96.1	70.1
F_{crit} (N)	890.2	875.0
F_{crit}* (N/g)	9.26	12.48
k_{comp} (N/mm)	236.4	224.1
k_{comp}* (N/g-mm)	2.46	3.20

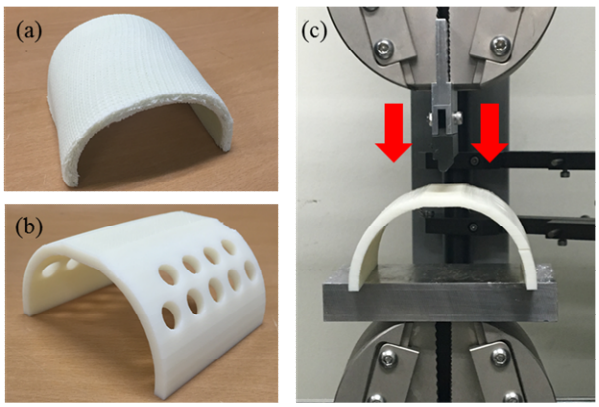

Fig. 11. Compression test for half-cylindrical shells: (a) Plaster shell; (b) 3d-printed ABS shell; (c) experimental setup.

sive stiffness (k_{comp}) were compared. The compressive stiffness was determined by measuring the slope of force-displacement curve in the linear elastic range. Table 5 compares the resulting critical force and stiffness of both structures. It can be seen that the critical force of the porous ABS shell (875.0 N) was slightly smaller than that of the plaster shell (890.2 N). However, the specific critical force (F_{crit}^*) per unit mass shows opposite results; the ABS shell shows a higher value (12.48 N/g) than the plaster case (9.26 N/g). A similar trend was observed in the case of the compressive stiffness (k_{comp}) and the specific compressive stiffness (k_{comp}^*); the absolute stiffness of the ABS shell was slightly lower than that of the plaster shell while their specific values showed opposite results. These results indicate that the porous ABS shell provides higher specific stiffness and strength in comparison with the plaster shell.

5. Conclusions

In this study, a porous cast for an elbow orthosis was developed to replace the traditional plaster casts. To develop a porous cast efficiently, various approaches including 3d scanning, 3d design with automatic hole generation, FE analyses, and AM were connected effectively. The 3d scanning was used to obtain the geometry of a human arm so that a customized cast fit to a human body could be designed. The automatic hole generation algorithm was developed to reduce the lead time of porous structure design (less than 10 minutes), enough to be applicable in point of care. FE analyses were performed to evaluate the bending stiffness of the porous cast and to suggest appropriate reinforcement structures that could compensate the stiffness degeneration due to porosity. AM was then used to fabricate the porous cast with a complicated geometry in a day.

Through these approaches, a customized porous cast was developed successfully and validated through experiments. Compared to traditional plaster casts, this porous cast has many advantages including lightweight structure, good ventilation, X-ray transparency, and better appearance. Further study is required to implement the developed porous cast on clinical trials in orthopedic treatments.

Acknowledgment

This study was supported by a grant from the Technology Innovation Program (Grant no: 10062348) funded by the Ministry of Trade, Industry & Energy (MOTIE, Korea).

Nomenclature

l : Length of the reinforcement rib
w : Width of the reinforcement flange
m : Mass of a cast
k* : Specific bending stiffness of a porous cast
k_{comp} : Compressive stiffness of a shell structure
k_{comp}* : Specific compressive stiffness of a shell structure
F : Amount of an external force
F_{crit} : Critical compressive force at failure
F_{crit}* : Specific critical force per unit mass
δ_{max} : The maximum deflection of a cast

References

[1] I. Campbell, D. Bourell and I. Gibson, Additive manufacturing: Rapid prototyping comes of age, *Rapid Prototyping J.*, 18 (4) (2012) 225-258.
[2] C. M. B. Ho, S. H. Ng and Y. J. Yoon, A review on 3D printed bioimplants, *Int. J. Precis. Eng. Manuf.*, 16 (5) (2015) 1035-1046.
[3] R. K. Chen, Y. A. Jin, J. Wensman and A. Shih, Additive manufacturing of custom orthoses and prostheses—A review, *Additive Manufact.*, 12 (2016) 77-89.
[4] M. T. Fitch, B. A. Nicks, M. Pariyadath, H. D. McFinnis and D. E. Manthey, Basic splinting techniques, *New England J. Medicine*, 359 (26) (2008) e32.
[5] M. C. Faustini, R. R. Neptune, R. H. Crawford and S. J. Stanhope, Manufacture of passive dynamic ankle-foot orthoses using selective laser sintering, *IEEE Trans. Biomed. Eng.*, 55 (2) (2008) 784-790.
[6] D. Cook, V. Gervasi, R. Rizza, S. Kamara and X. C. Liu, Additive fabrication of custom pedorthoses for clubfoot correction, *Rapid Prototyping J.*, 16 (3) (2010) 189-193.
[7] C. Mavroidis, R. G. Ranky, M. K. Sivak, B. L. Patritti, J. DiPisa, A. Caddle, K. Filhooly, L. Govoni, S. Sivak, M. Lancia, R. Drillio and P. Bonago, Patient specific ankle-foot

orthoses using rapid prototyping, *J. Neuroeng. Rehabil.*, 8 (1) (2011) 1-11.
[8] D. Palousek, J. Rosicky, D. Koutny, P. Stoklásek and T. Navrat, Pilot study of the wrist orthosis design process, *Rapid Prototyping J.*, 20 (1) (2014) 27-32.
[9] H. Kim and S. Jeong, Case study: Hybrid model for the customized wrist orthosis using 3D printing, *J. Mech. Sci. Technol.*, 29 (12) (2015) 5151-5156.
[10] A. M. Paterson, R. Bibb, R. I. Campbell and G. Bingham, Comparing additive manufacturing technologies for customised wrist splints, *Rapid Prototyping J.*, 21 (3) (2015) 230-243.
[11] CORTEX, *http://www.evilldesign.com/cortex*.
[12] OSTEOID, *http://www.osteoid.com*.
[13] H. Ko, S. K. Moon and K. Hwang, Design for additive manufacturing in customized products, *Int. J. Precis. Eng. Manuf.*, 16 (11) (2015) 2369-2375.
[14] M. K. Thompson, G. Moroni, T. Vaneker, G. Fadel, R. I. Campbell, I. Gibson and F. Martina, Design for additive manufacturing: trends, opportunities, considerations, and constraints, *CIRP Annl. Manuf. Technol.*, 65 (2) (2016) 737-760.
[15] S. Jang, C. H. Goh and H. J. Choi, Multiphase design exploration method for lightweight structural design: Example of vehicle mounted antenna-supporting structure, *Int. J. Precis. Eng. Manuf. Green Tech.*, 2 (2) (2015) 281-287.
[16] C. Chu, G. Graf and D. W. Rosen, Design for additive manufacturing of cellular structures, *Computer-Aided Design Appl.*, 5 (5) (2008) 686-696.
[17] J. Chu, S. Engelbrecht, G. Graf and D. W. Rosen, A comparison of synthesis methods for cellular structures with application to additive manufacturing, *Rapid Prototyping J.*, 16 (4) (2010) 275-283.
[18] D. J. Yoo, New paradigms in cellular material design and fabrication, *Int. J. Precis. Eng. Manuf.*, 16 (12) (2015) 2577-2589.
[19] X. Y. Kou and S. T. Tan, A simple and effective geometric representation for irregular porous structure modeling, *Computer-Aided Design,* 42 (10) (2010) 930-941.
[20] D. J. Yoo and K. H. Kim, An advanced multi-morphology porous scaffold design method using volumetric distance field and beta growth function, *Int. J. Precis. Eng. Manuf.*, 16 (9) (2015) 2021-2032.
[21] W. Wang, T. Y. Wang, Z. Yang, L. Liu, X. Tong, W. Tong, J. Deng, F. Chen and X. Liu, Cost-effective printing of 3D objects with skin-frame structures, *ACM Trans. Graph.*, 32 (6) (2013) 177.
[22] L. Lu, A. Sharf, H. Zhao, Y. Wei, Q. Fan, X. Chen, Y. Savoye, C. Tu, D. Cohen-Or and B. Chen, Build-to-last: Strength to weight 3D printed objects, *ACM Trans. Graph.*, 33 (4) (2014) 97.
[23] Y. E. Lim and K. Park, Investigation of bending stiffness of porous shell structures fabricated by 3D printing, *Trans. KSME (A),* 41 (6) (2017) 491-497.
[24] J. Cho, J. Koo and H. Jung, A lightweight design approach for an EMU carbody using a material selection method and size optimization, *J. Mech. Sci. Technol.*, 30 (2) (2016) 673-681.

Yeong-Eun Lim is a master candidate in the Department of Mechanical Design and Robot Engineering at Seoul National University of Science and Technology, Korea. She received a B.S. from Seoul National University of Science and Technology in 2015. Her current research includes design and analysis of lightweight structure for additive manufacturing.

Keun Park received his B.S. and M.S. degrees in Precision Engineering and Mechatronics from KAIST, Korea, in 1992 and 1994, respectively. He then received his Ph.D. degree in Mechanical Engineering from KAIST in 1999. Dr. Park is currently a Professor of the Department of Mechanical System Design Engineering at Seoul National University of Science and Technology, Korea. His research interests include numerical analysis of material forming processes, micro-fabrication, and additive manufacturing.